J Mater Sci (2007) 42:8652–8661
DOI 10.1007/s10853-007-1828-y

Damage evaluation of refractories under cyclic loading–unloading processes using ultrasonic method

Ryoichi Furushima · Yohtaro Matsuo · Tadashi Shiota · Kouichi Yasuda

Received: 28 March 2006 / Accepted: 8 May 2007 / Published online: 4 July 2007

Abstract Accumulation of damage by cyclic loading–unloading under uni-axial compressive stress was evaluated using ultrasonic method for two kinds of refractories: alumina/graphite (AG) and isotropic graphite (IG) refractories. Change of relative degradation in apparent sonic velocity V_{RD} was used for a barometer on damage evaluation of IG and AG refractories. Measurement of change in V_{RD} actualizes in-situ evaluation of damage during loading–unloading processes. Difference of change in V_{RD} during loading–unloading processes was observed between both specimens, which suggested the damage mechanism is different in IG and AG. Accumulation of damage for AG specimens by cyclic loading–unloading was very little, while it is a little larger for IG specimens. An increase in applied stress ratio R contributed to an increase in degree of damage accumulation. To explain the damage mechanism for both AG and IG specimens, we consider damage models, respectively. In these models, loading–unloading processes were classified into 4 steps based on the behavior of change in V_{RD}, and damage of the two kinds of specimens was explained by relating to crack nucleation and crack opening-closing mechanism in each step.

Introduction

In the field of steel industry, a large amount of refractories are used for such as convectors, teeming ladles, electric furnaces, and so on. Since most of these refractories are used under high temperature condition, they are frequently subjected to the thermal shock by which damage is induced (so called thermal spalling). So far there are many studies on this type of damage from the standpoint of stable operation in the industry [1–5].

In addition to the thermal shock damage, these refractories are damaged by thermal stress originating from a temperature gradient if they are subjected to mechanical constraint. In a compressively stressed region of refractories such as lining bricks, this mechanical damage accumulates due to cyclic thermal loading–unloading.

Figure 1 shows a schematic drawing of a ladle in which the refractories used for lining are located between molten steel and an iron shell. These refractories facing on the molten steel are subjected to compressive stress. By this stress they are damaged repeatedly whenever molten steel is poured into the empty ladle cyclically. Therefore, this cyclic mechanical damage has been recognized as a significant problem as well as the thermal shock damage in order to maintain the reliability of refractories. However, few studies have been performed on this mechanical damage of refractories due to the compressive stress and/or the cyclic compressive loading–unloading.

Many works on the damage evaluation have been reported based on the various viewpoints such as remaining life [6], microstructure (defects) [7], changing physical parameters [8, 9] or thermodynamic potential [10, 11], since damage can not directly measurable. Ultrasonic method is known as one of the indirect measurement procedures. The merit of ultrasonic method is simple and easy to measure the acoustic parameters such as apparent sonic velocity and attenuation coefficient. From these parameters, Young's modulus, which is a typical barometer on damage of a measured material, can be calculated. Using

R. Furushima (✉) · Y. Matsuo · T. Shiota · K. Yasuda
Department of Metallurgy and Ceramic Science, Tokyo Institute of Technology, 2-12-1 Ookayama, Meguro-ku, Tokyo 152-8552, Japan
e-mail: rfurushima@eng.ceram.titech.ac.jp

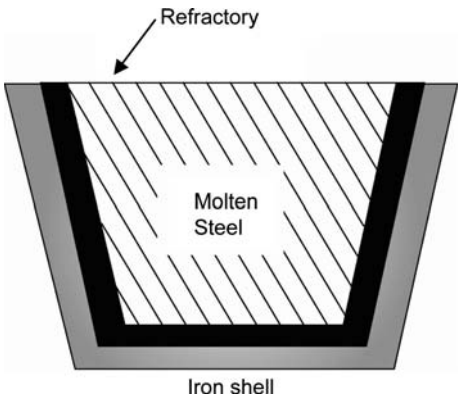

Fig. 1 A schematic illustration of a ladle

change in these acoustic parameters, the damage evaluation of C/SiC composite was reported [12].

The purpose of this paper is to detect and characterize the mechanical damage process in refractories during the uni-axial compression tests. Using ultrasonic method, the change in apparent sonic velocity was measured during loading–unloading processes for two kinds of refractories. From the results of change in the apparent sonic velocity by cyclic loading–unloading, damage accumulation was evaluated, and damage mechanism during loading–unloading processes was considered for these two refractories.

Experimental procedure

Samples

The refractories used in this study are alumina/graphite (AG) and isotropic graphite (TOYO TANSO, IG12, hereafter IG) refractories. The main chemical composition of an AG refractory is shown in Table 1. AG specimens (40 mm in width, 40 mm in height and 10 mm in thickness) were cut from an AG refractory block. The IG specimens (30 mm in width, 30 mm in height and 10 mm in thickness) were also cut from one big block. Table 2 gives the data on physical and mechanical properties for both AG and IG specimens.

Table 1 Chemical composition of an AG refractory

Composition	Volume fraction / %
Al_2O_3	27
C	27
SiO_2	19
SiC	5
ZrO_2	1

Cyclic loading–unloading tests under uni-axial compressive stress

Cyclic uni-axial compressive loading–unloading tests were carried out on two kinds of specimens using an Insron type testing machine (JT TOHSHI Co. Ltd., SC-100H type). A strain gage was glued on the surface of each specimen whose normal is perpendicular to the loading axis. The maximum number of loading–unloading cycle was 50 and crosshead speed 0.1 mm/min. In order to normalize the effect of the maximum compressive stress on damage of refractories, applied stress ratio R is defined as

$$R \equiv \frac{\sigma_M}{\tilde{\sigma}_f} \quad (1)$$

where σ_M denotes the maximum applied compressive stress and $\tilde{\sigma}_f$the mean fracture stress as shown in Table 2. We set R to three levels: 0.5, 0.7 and 0.9 for both IG and AG specimens. The compressive stress was calculated from dividing the load by the area of cross section. Strain data were obtained directly from the strain gage signal.

Ultrasonic method for measuring apparent sonic velocity

Ultrasonic measurements under uni-axial compressive loading–unloading tests were carried out on both AG and IG specimens using an instrument for elastic modulus measurement (Toshiba Tungaloy, UMS-H). A transducer which has the performance to transmit, and receive the longitudinal sonic waves (Toshiba Tungaloy) was mounted on one side face of a specimen. Nominal frequency was set to 1.0 MHz in which S/N ratio was sufficiently so large that the least error originating from noise was expected. A schematic illustration of the measuring system is shown in Fig. 2. The received waves were digitized and then analyzed using software called ''Sonic Scope'' (Toshiba Tungaloy).

Figure 3 shows an example of observed longitudinal sonic waves monitored by a personal computer. The first and the second echoes which reflected once and twice on

Table 2 Physical and mechanical properties for IG and AG refractories

	IG	AG
Bulk density/g cm^{-3}	1.78	2.23
Apparent density/g cm^{-3}	2.05	2.76
True density/g cm^{-3}	2.11	2.81
Total porosity/%	15.6	20.6
Fracture stress/MPa	94	25
Young's modulus/GPa	10	9

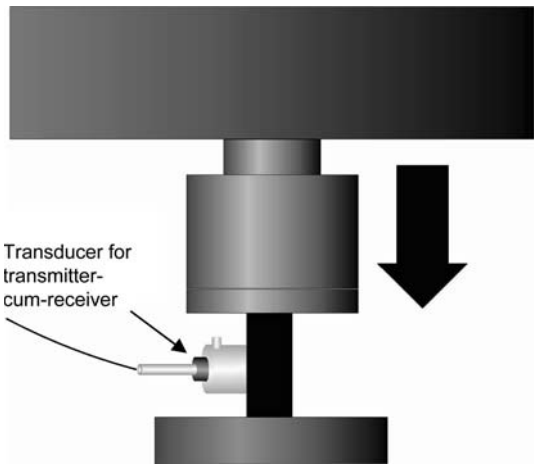

Fig. 2 A schematic illustration of uni-axial compression tests accompanied by ultrasonic measurement

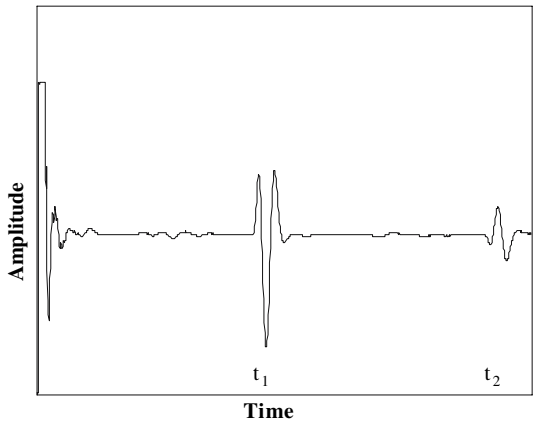

Fig. 3 Observed longitudinal waves obtained by ultrasonic method

the opposite surface opposite to the incident surface, respectively. The former waves were referred as first echo wave and the latter as second echo wave.

Apparent sonic velocity V_A was determined by the time interval $(t_2 - t_1)$ as the following equation (see Fig. 3),

$$V_A = \frac{2L}{t_2 - t_1} \tag{2}$$

where L denotes the specimen width, t_1 and t_2 the times corresponding to the first echo wave and the second echo wave, respectively.

As an acoustic parameter for damage evaluation, we introduced relative degradation in apparent sonic velocity V_{RD} obtained form V_A as follows,

$$V_{RD} \equiv \frac{V_{A0} - V_A}{V_{A0}} \tag{3}$$

where V_{A0} denotes apparent sonic velocity before first loading.

Experimental results

Stress–strain curves

Figures 4a–c and 5a–c show the effect of applied stress ratio R on stress–strain curves for AG and IG specimens, respectively. It is noted that the IG specimen of R = 0.9 was fractured during 48th loading–unloading cycle.

Each of these curves has a non-linear part in loading processes due to quasi-elastic-plastic deformation and has a hysteresis loop. The cumulative residual strain ε_R increases with the number of loading–unloading cycle, while the incremental of residual strain decreases with the number of cycle. Change in R not only affects the maximum strain or residual strain, but also affects the degree of non-linearity during unloading processes. For example, the curvature of a stress–strain curve during the unloading process decreases with an increase in R.

Change in the ratio of hysteresis loop area

The ratio of hysteresis loop area R_{hys} is obtained from in each number of cycles to that in the first cycle. The effects of R on ratio of hysteresis loop area R_{hys} are shown in Fig. 6a for AG specimens and Fig. 6b for IG specimens. In general, the formation of a hysteresis loop is caused by the dissipation of energy due to slip at interfaces of some kinds of grains [12]. So, R_{hys} can be used for the barometer of change in inner microstructure for both specimens. As shown in Fig. 6, R_{hys} for each R starts decreasing rapidly and approaches to each constant value as the number of loading–unloading cycle increases for both specimens. This means that the degrees of slip at the interfaces of grains become steady with an increase in loading–unloading cycle.

About the effect of R on R_{hys}, there is explicit difference between both specimens. In the case of AG specimens, there is little difference of R_{hys} between R = 0.5 and R = 0.7, while R_{hys} shifts to higher value from R = 0.7 to R = 0.9. On the other hand, in the case of IG specimens, R_{hys} shifts to higher value with an increase in R, which indicates that the more maximum compressive stress increases, the more microstructural change in the IG specimen occurs by cyclic loading–unloading. The microstructural change is one of the most important factors to consider damage of materials. The larger microstructural change may lead to the higher degree of damage. From the comparison between Fig. 6a and b, the values of R_{hys} for IG specimens are higher than those for AG specimens.

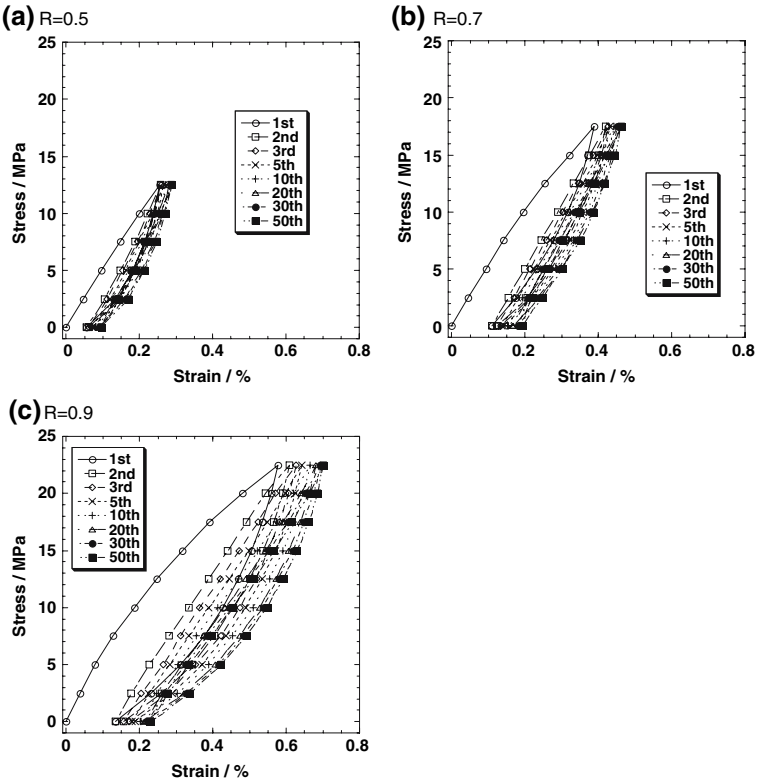

Fig. 4 The effect of applied stress ratio R on stress stress–strain curves for AG specimens

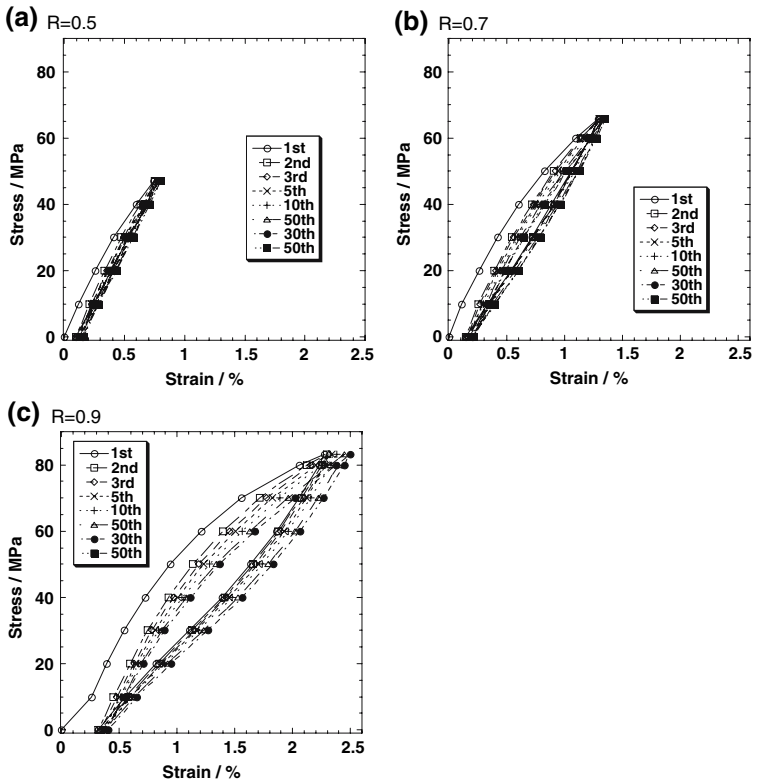

Fig. 5 The effect of applied stress ratio R on stress stress–strain curves for IG specimens

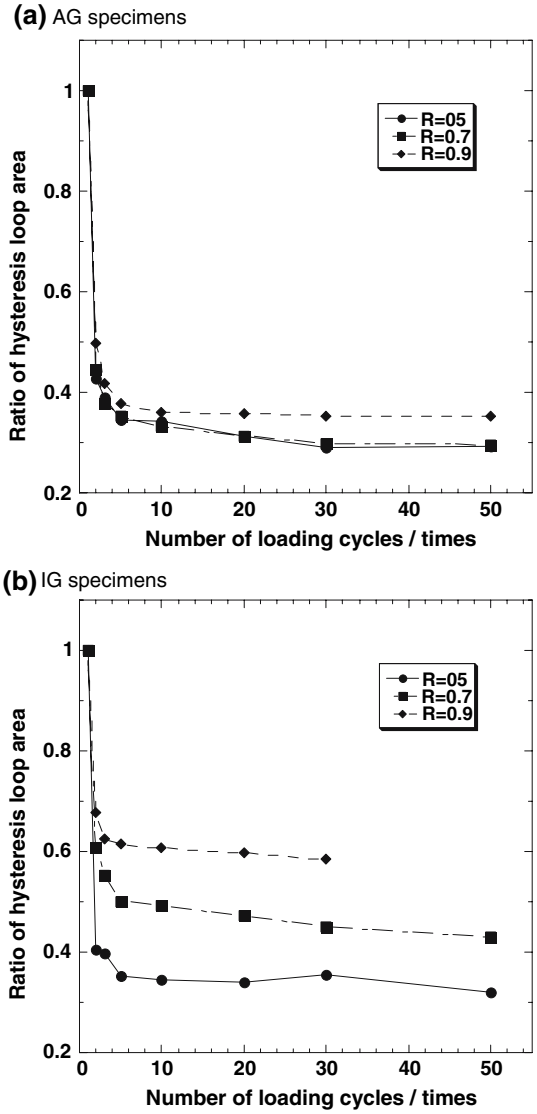

Fig. 6 The effect of R on ratio of hysteresis loop area R_{hys}

Thus, the damage accumulation for IG specimens is considered to be larger than that for AG specimens at relatively high applied stress ratio.

Change in apparent sonic velocity

The effect of applied stress ratio R on the relative degradation in apparent sonic velocity V_{RD} for AG and IG specimens are shown in Figs. 7 and 8. In both cases, the behavior of V_{RD} change is strongly influenced by the stress ratio R, and besides, the behavior of V_{RD} change in the first cycle is quite different from the subsequent cycles.

In the first cycle for AG specimens, V_{RD} increases during the loading process, while during the unloading process, it further increases monotonically until the complete unloading. On the contrary, in the first cycle for IG specimens, V_{RD} increases during the loading process, while during the unloading process, V_{RD} vs stress curve shows concave. In the subsequent cycles for AG specimens, V_{RD} decreases during a loading process whereas in an unloading process, it increases along almost the same trace in the loading one. In the subsequent cycles for IG specimens, V_{RD} vs stress curve shows concave.

The total increment of V_{RD} for each R in both specimens increases with the number of loading–unloading cycle, while the increment in one cycle decreases as the number of cycle increases. In the 50th cycle, the increment of V_{RD} in one cycle is very little.

Discussions

Dependence of the number of loading–unloading cycle on V_{RDf} and ε_R

The dependence of the number of loading–unloading cycle on change in the relative degradation in apparent sonic velocity V_{RD} in one loading–unloading cycle (=V_{RDf}) and the cumulative residual strain (=ε_R) are shown in Fig. 9 for AG specimens and in Fig. 10 for IG specimens, respectively. It is found that V_{RDf} and ε_R start increasing followed by a slow approach to saturation as the number of loading–unloading cycle increases for both specimens. This indicates that damage of specimens by several loading–unloading cycles at early cycles is larger than that by the subsequent loading–unloading cycles.

Comparing Fig. 9 with Fig. 10, it is found that the saturation rates of V_{RDf} for AG specimens are faster than that for IG specimens despite of a similar saturation rate of ε_R between AG and IG specimens. The former result suggests that damage accumulation by cyclic loading–unloading for IG specimens is larger than that of AG specimen. More concretely, AG specimens mainly damaged by the first loading–unloading cycle; however, they are much less damaged by the subsequent loading–unloading cycles. On the other hand, damage of IG specimens by the first loading–unloading cycle is less than that of AG specimens whereas damage of IG specimens by the subsequent loading–unloading cycles is more than that of AG specimens. It is noted that both V_{RDf} and ε_R for the IG specimen with R = 0.9 continue increasing even at 30 cycles, which means that damage of this specimen accumulates even over 30 cycles by cyclic loading–unloading. In fact, this specimen fractured at 48th cycle.

Dependence of ratio of applied stress R on V_{RDf} and ε_R

The dependence of the ratio of applied stress R on V_{RDf} and ε_R are shown in Fig. 11 for AG specimens and in Fig. 12 for IG specimens. V_{RDf} and ε_R increases with an

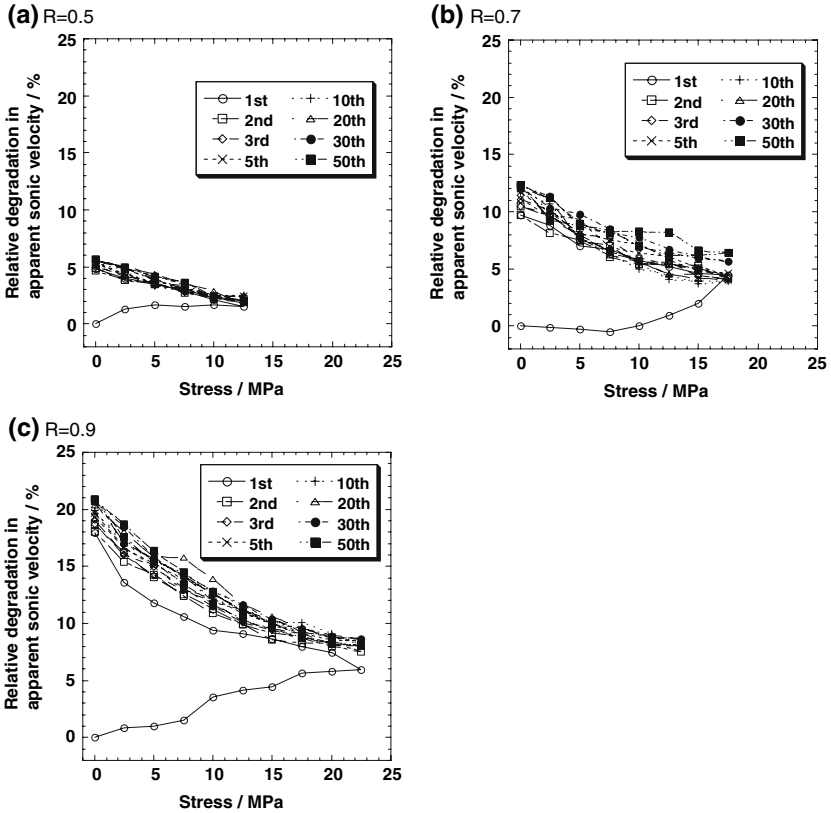

Fig. 7 The effect of R on relative degradation in apparent sonic velocity V_{RD} for AG specimens

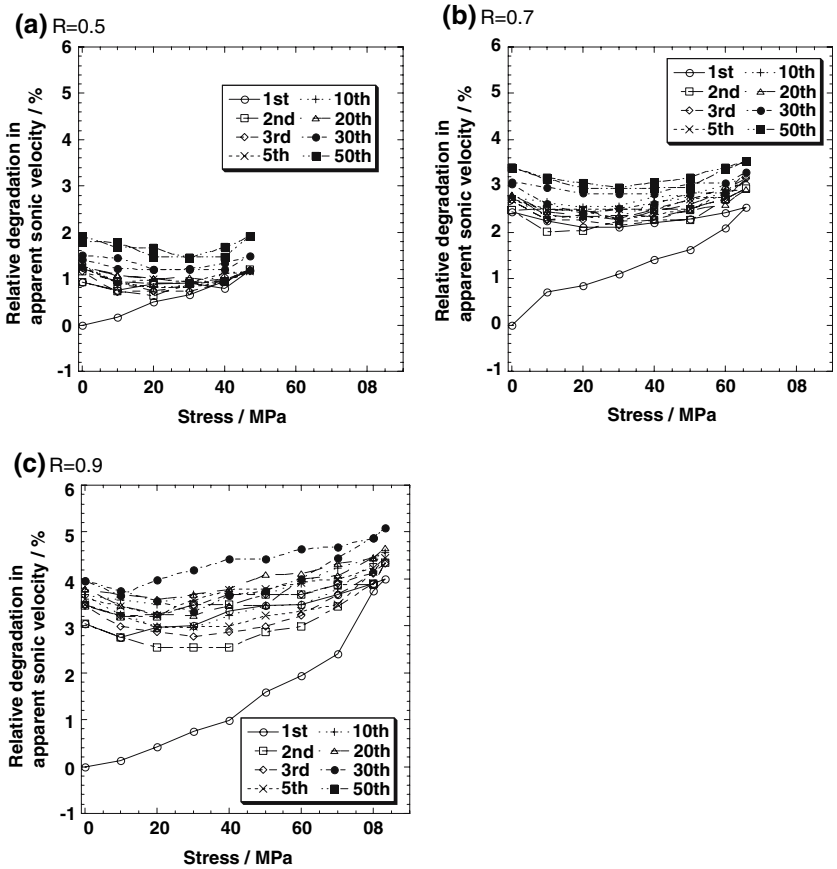

Fig. 8 The effect of R on relative degradation in apparent sonic velocity V_{RD} for IG specimens

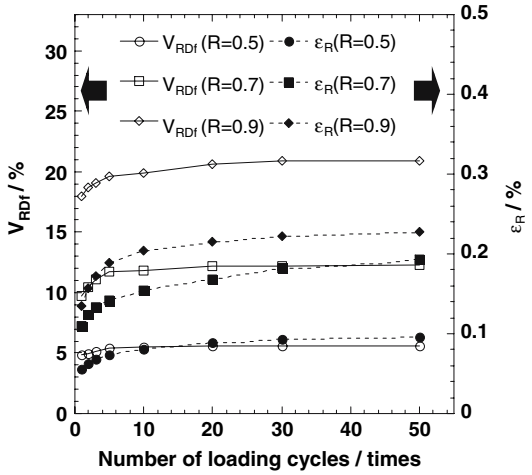

Fig. 9 The dependence of the number of loading–unloading cycle on change in V_{RD} in one loading–unloading cycle (=V_{DRf}) and the cumulative residual strain (=ε_R) for AG specimens

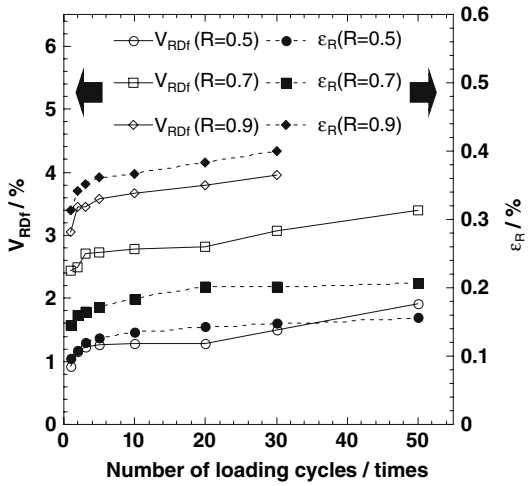

Fig. 10 The dependence of the number of loading–unloading cycle on change in V_{RD} in one loading–unloading cycle (=V_{DRf}) and the cumulative residual strain (=ε_R) for IG specimens

increase in R for both kinds of specimens. However, the effect of number of loading–unloading cycles on V_{RDf} and ε_R is not large.

Damage models for AG and IG specimens

From the results of change in V_{RD} shown in Figs. 7 and 8, we propose damage models for AG and IG specimens, respectively. Each damage model is classified into 4 steps: first loading process, first unloading process, subsequent loading processes and subsequent unloading processes. We referred these steps as Step1, Step2, Step3 and Step4 in turn.

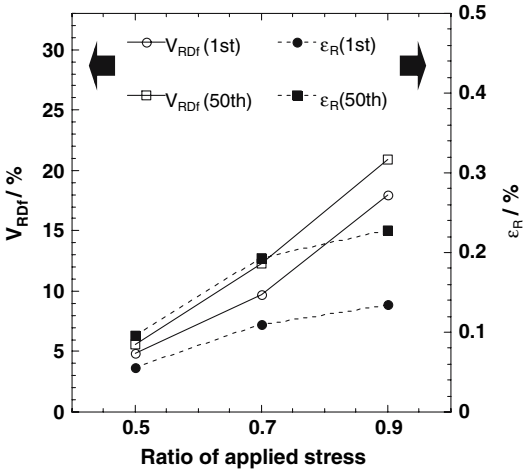

Fig. 11 The dependence of the applied stress ratio R on V_{RDf} and ε_R for AG specimens

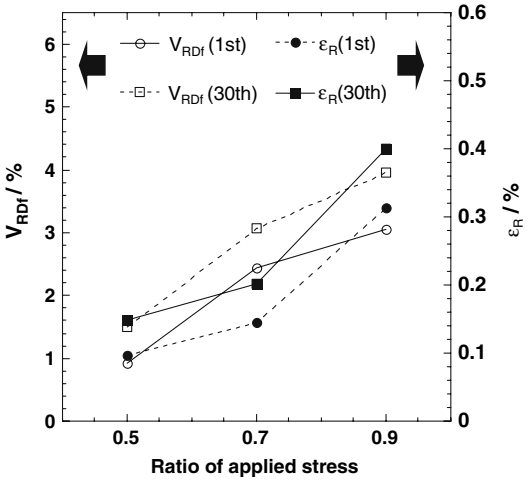

Fig. 12 The dependence of the applied stress ratio R on V_{RDf} and ε_R for IG specimens

Damage model for AG specimens

In the case of AG specimens, a characteristic behavior is observed; V_{RD} increases during unloading processes. This means the specimen is damaged during unloading processes. However, this damage is considered to be almost recovered during loading processes except the first loading process. Therefore, we call this damage ''apparent reversible damage'' which is opposed to ''irreversible damage'' due to accumulation of small damage by each loading–unloading cycle. These two types of damage should be included in the damage model for AG specimens.

A virgin AG specimen contains alumina particles, graphite matrix and some silica phase. In the damage model, we assume that alumina particles are dispersed in graphite matrix in order to simplify the system (Fig. 13a).

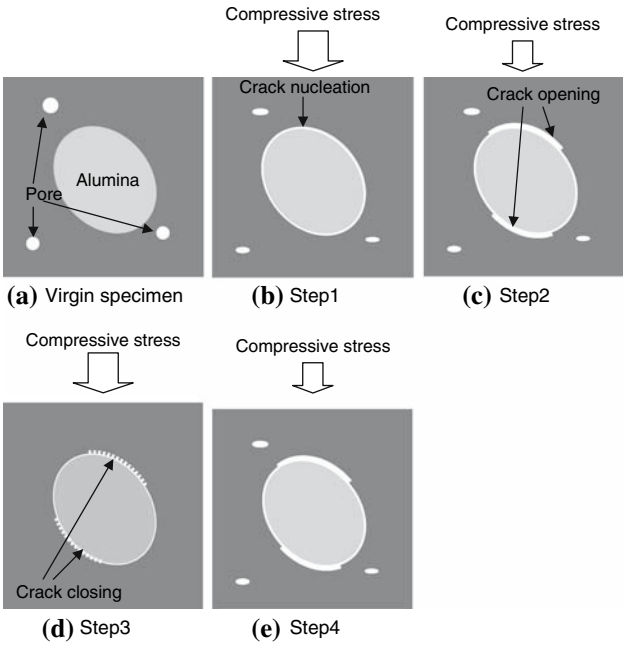

Fig. 13 Damage model for AG specimen (**a**) Virgin specimen, Alumina particles are dispersed in graphite matrix. (**b**) Step1, New cracks at interfaces between alumina particles and graphite matrix nucleate accompanied by collapse of pores and quasi-plastic deformation in softer graphite matrix part. (**c**) Step2, Cracks locating at interfaces between alumina particles and graphite matrix open and slightly extend. (**d**) Step3, The interfacial cracks close. (**e**) Step4, The interfacial cracks open and a little extend again

During Step1, stress concentrations are induced by mismatch of deformation at the interfaces between alumina particles and graphite matrix. Therefore, new cracks might nucleate at these interfaces accompanied by shrinkage of pores and quasi-plastic deformation in softer graphite matrix part (Fig. 13b). During this step, the specimen is subjected to the irreversible damage, which causes the increase in V_{RD}. During Step2 (first unloading), cracks locating at the interfaces open and slightly extend (Fig. 13c). This mechanism is similar to the local re-yielding of metal during unloading process [13] after large-scale plastic deformation. Because of this crack opening and extending mechanism, which causes the damage, V_{RD} further increases steeply. During Step3 (subsequent loading), these cracks locating at the interface close (Fig. 13d), so V_{RD} increases again along the similar trace in Step2. It is noted that the crack opening occurred in Step2 and the crack closing in Step3 correspond to ''apparent reversible damage'' mentioned previously. During Step4, these cracks open and a little bit extend again (Fig. 13e). This mechanism is similar to that of Step2. Therefore, V_{RD} increases along the similar trace in Step2 and Step3.

In addition to the above damage mechanism, accumulation of the irreversible damage exists due to cyclic loading–unloading. Thus, the trace in Step2 or Step4 is almost the same as that in Step3; but it is not completely the same. Thus the overall damage mechanism for AG specimens can be explained using the above damage model.

Damage model for IG specimens

In the case of IG specimens, both an increase and a decrease in V_{RD} are found during a loading or unloading cycle except the first loading process. This behavior indicates that the two types of damage mechanism, namely ''apparent reversible damage'' and irreversible damage, are included in one process. To explain the two opposite damage mechanisms, we assume two types of preexisting crack: a longitudinal type and a lateral type. Longitudinal-type cracks incline slightly to the loading direction whereas lateral-type cracks lie almost perpendicular to the loading direction. For the sake of simplicity, we suppose a two-dimensional model in which these cracks are located at interfaces among graphite particles consisting of assemblies of regular hexagonal crystals (Fig. 14a). These two types of cracks present the opposite behavior against uniaxial loading–unloading. When the longitudinal-type cracks open, the lateral-type cracks close, and vice versa.

During Step1, new longitudinal-type cracks are nucleated. In addition, the intrinsic longitudinal-type cracks open and extend, while the lateral-type cracks close (Fig. 14b). Since the incident plane waves propagate perpendicular to the loading direction in our experiment, opening and extending of the longitudinal-type cracks highly contribute to an increase in scattering cross-section. On the contrary, closing of the lateral-type cracks hardly contributes to decrease in scattering cross-section. Therefore, if the applied stress is sufficiently large, opening and extending of the longitudinal-type cracks contribute the increase in V_{RD} as well as the crack nucleation. Thus, during Step1, the specimen is damaged due to the nucleation of new longitudinal-type cracks and opening and extending of the intrinsic longitudinal-type cracks. During Step2, the longitudinal-type cracks close and the lateral-type cracks re-open (Fig. 14c). At high compressive stress region over about 20 MPa, the effect of closing the longitudinal-type cracks on a decrease in V_{RD} is higher than that of re-opening the lateral-type cracks on an increase in V_{RD}. Therefore, V_{RD} decreases during the high stress region. At the lower compressive stress region from 20 MPa to 0 MPa, the effect of re-opening the lateral-type cracks is higher than that of closing the longitudinal- type cracks. Hence, V_{RD} increases during the low stress region. During Step3, the longitudinal-type cracks open and the lateral-type cracks close again (Fig. 14d). Up to 20 MPa the effect of closing the lateral-type cracks on a decrease in

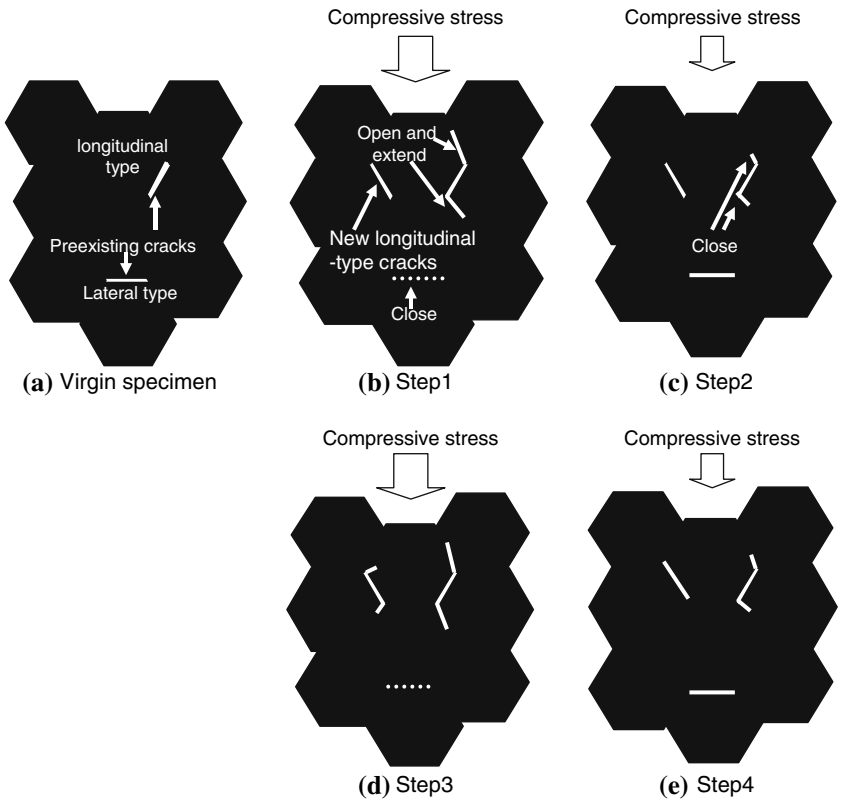

Fig. 14 Damage model for IG specimens (**a**) Virgin specimen, There are two types of preexisting crack: longitudinal type and lateral type. (**b**) Step1, New longitudinal-type cracks are nucleated and the intrinsic longitudinal-type cracks open and extend, while the lateral-type cracks close. (**c**) Step2, The longitudinal-type cracks close and the lateral-type cracks open. (**d**) Step3, The longitudinal-type cracks open and the lateral-type cracks close again. (**e**) Step4, The longitudinal-type cracks close and the lateral-type cracks open again

V_{RD} is higher since the stress is not high enough to open the longitudinal-type cracks. Over 20 MPa opening of the longitudinal-type cracks causes increase in V_{RD}. Thus, V_{RD} decreases up to 20 MPa and then it increases up to the maximum stress along the similar trace in Step2. During Step4, the longitudinal-type cracks close and the lateral-type cracks open again (Fig. 14e). Since this mechanism is the same as that of Step2, V_{RD} decreases up to 20 MPa and then it increases along the similar trace in Step2 and Step3.

Similar to the case of the AG specimen, the IG specimens are subjected to accumulation of the irreversible damage due to the cyclic loading–unloading. However, the amount of damage accumulation for IG specimens is a little larger than that for AG specimens. Thus, the trace of V_{RD} in Step3 and Step4 is shifted to higher value by degrees as the number of loading–unloading cycle increases. Thus, the overall damage mechanism for IG specimens can be explained using the above model.

Conclusions

In this paper, accumulation of damage by cyclic loading–unloading under uni-axial compressive stress was evaluated using ultrasonic method for two kinds of refractories: alumina/graphite (AG) and isotropic graphite (IG) refractories. Change of relative degradation in apparent sonic velocity V_{RD} was used for a barometer on damage evaluation of IG and AG refractories as well as stress–strain curves.

Though there was not apparent difference on the behavior of stress–strain curves between AG and IG specimen, apparent difference of change behavior in V_{RD} was observed. This difference was attributed to that of damage mechanism during loading–unloading processes between them. An increase in applied stress ratio R contributed to an increase in degree of damage accumulation. However, similar diagram of change in V_{RD} for each R was observed, which indicated that damage mechanism was not influenced by change in R.

From the results of change in V_{RD} during loading–unloading processes for the two kinds of specimens, it was found that the damage mechanism could be classified into four steps: first loading process, first unloading process, subsequent loading processes and subsequent unloading processes for each specimen. Each step has a different damage mechanism, which includes nucleation and extending of cracks and crack opening-closing mechanism. The former may be regarded as irreversible damage, while the latter as ‘‘apparent reversible damage’’. The accumulation of irreversible damage for IG specimens by cyclic loading–unloading was a little larger than that for AG specimens.

References

1. Lee WJ, Case ED (1989) Mater Sci Eng A119:113
2. Lee WJ, Case ED (1990) J Mater Sci 25:5043
3. Kim Y et al (1990) The minerals, metals and materials society, p 479
4. Kim Y et al (1990) Proceedings of the American society for composites, 5th technical conference, p 871
5. Schmitt N et al (2002) Mech Mater 34:725
6. Manson SS (1979) ICM 3, Cambridge 1:13
7. Dyson VD, McLean D (1977) Met Sci 2:37
8. Jonas JJ, Baudelet B (1977) Acta Metallur 25:43
9. Bui-Quoc T et al (1971) J Basic Engng Trans ASME, p 691
10. Sidoroff F (1975) Arch Mech Poland 27(5–7):807
11. Germain P et al (1983) ASME J Appl Mech 50:1010
12. El Bouazzaoui R, Baste S, Camus C (1996) Comp Sci Technol 56:1373
13. Yoshida F et al (2002) Int J Plasticity 18:661